NUMERICAL ANALYSIS OF SOME PROBLEMS RELATED TO THE MECHANICS OF PNEUMATIC TIRES: FINITE DEFORMATION/ROLLING CONTACT OF A VISCOELASTIC CYLINDER AND FINITE DEFORMATION OF CORD-REINFORCED RUBBER COMPOSITES*

J. Tinsley Oden and Eric B. Becker
and
T.L. Lin and K.T. Hsieh
The University of Texas at Austin
Austin, Texas

SUMMARY

The formulation and numerical analysis of several problems related to the behavior of pneumatic tires are considered. These problems include the general rolling contact problem of a rubber-like viscoelastic cylinder undergoing finite deformations and the finite deformation of cord-reinforced rubber composites. New finite element models are developed for these problems. Numerical results obtained for several representative cases are presented.

INTRODUCTION

The study of the behavior of pneumatic tires under various loading conditions constitutes one of the most challenging and difficult collections of nonlinear problems in the mechanics of solids. It is our aim in this paper to investigate two subclasses of problems related to tire mechanics which encompass some significant and complex features of tire behavior:

1) The general rolling contact problem of finite deformation of a flexible, viscoelastic cylinder in steady-state motion on a rough foundation (roadway)

2) The finite deformation of cord-reinforced rubber composites

---

* The work reported here was supported by the NASA Langley Research Center under Contract NAS1-17359 as a part of the National Tire Modelling Program, with the Computational Mechanics Co., Inc. The encouragement and support of this work by Mr. John Tanner of NASA is gratefully acknowledged.

In all of the formulations considered here, we place no limitations on the order of magnitude of deformations; if strains are "small or moderate", as is sometimes the case in cord-reinforced tires, then the prediction of small or moderate strains should be a natural outcome of our analysis. Moreover, we also incorporate the effects of non-conservative loads such as those encountered in the pressurization of flexible surfaces.

For problem class 1, the rolling contact problem, we present a new and general variational principle governing steady-state rolling of a cylindrical body, with finite deformations, unilateral contact, friction, viscoelastic response, and possibly standing waves at certain critical angular velocities. This principle involves a highly nonlinear variational inequality with the motion of the cylinder relative to a natural reference configuration as the unknown. This variational principle represents a generalization of our earlier work (ref. 1) to viscoelastic materials, viscoelastic effects being included to provide a model of rolling resistance in tires. We use this variational principle, or rather a regularized form of it, as a basis for the development of two-dimensional finite element models. We discuss algorithms for solving the resulting systems of nonlinear equations, locating bifurcations and limit points, and following solution paths which are based on continuation methods of the Riks, Wempner, Keller type. Numerical solutions of several representative problems are presented.

For problem class 2, the finite deformation of cord-reinforced rubber composites, new finite element models are developed which employ anisotropic membrane elements to model the cord layer and quadratic isoparametric elements to model the rubber matrix. The rubber can be modelled as an incompressible or compressible material and Halpin-Tsai or Gough-Tangorra-type representations (see, e.g., ref. 2) can be used as a basis for the model of the cord layers. An interesting feature of such composite models is that they can predict the change in "optimum" ply angles with finite uniaxial stretching, a phenomenon well outside the scope of linear models of composite materials. Some representative numerical solutions are presented.

MECHANICS OF FINITE ROLLING CONTACT OF A VISCOELASTIC CYLINDER

Our first objective is to formulate the equations and inequalities governing the deformation of a cylindrical body rolling at a constant angular velocity ω on a rough rigid roadway, as indicated in figure 1. A key consideration is the kinematics: we compare the geometry of the deformed cylinder in its current configuration C with that of a rigid cylinder spinning at the same angular velocity ω, the latter characterizing the reference configuration C_0. Polar cylindrical coordinates (r, θ, z) of a particle with labels $(R, \textcircled{H}^0, Z)$ at some arbitrary reference time $\tau = 0$ are defined by

$$r = R \ , \ \theta = \textcircled{H} + \omega t \ , \ z = Z \quad (t \geq 0) \tag{1}$$

or, alternatively, we can employ the cartesian reference coordinates

$$X_1 = r \cos \theta \ , \ X_2 = r \sin \theta \ , \ X_3 = z \tag{2}$$

The reference coordinates (r, θ, z) or (X_1, X_2, X_3) are thus time dependent, but this dependence is only formal since the shape of the deformed cylinder is the same at all times t to any observer fixed to the axle of the cylinder. The geometry is illustrated in Figure 1.

The motion $\underset{\sim}{u}$ of the cylinder is defined by an invertible, twice differentiable map $\underset{\sim}{\chi}$ that takes the configuration C_0 into the configuration C.

In particular, the cartesian components of $\underset{\sim}{u}$ relative to the fixed spatial frame of reference are given by

$$u_i = \chi_i(r, \theta, z) = \bar{\chi}_i(X_1, X_2, X_3) \tag{3}$$

Thus, time enters our description of motion only implicitly as $\theta = H + \omega t$. Henceforth, we shall not distinguish between the values $\underset{\sim}{u}$ (or u_i) of the map $\underset{\sim}{\chi}$ and the map itself, unless confusion is likely.

With this kinematical convention, we can easily write down expressions for the deformation gradient $\underset{\sim}{F}$, the right (left) Cauchy-Green deformation tensor $\underset{\sim}{C}$ ($\underset{\sim}{B}$), the displacement field $\underset{\sim}{d}$, the velocity $\underset{\sim}{v}$, and the acceleration $\underset{\sim}{a}$:

$$\begin{aligned}
&\underset{\sim}{F} = \underset{\sim\sim}{\nabla u} \; ; \; F^{i}_{\cdot j} = \{\partial u_i / \partial X_j\} \\
&\underset{\sim}{C} = \underset{\sim}{F}^T \underset{\sim}{F} \; , \; \underset{\sim}{B} = \underset{\sim}{F} \; \underset{\sim}{F}^T \\
&\underset{\sim}{d} = \underset{\sim}{u} - \underset{\sim}{r} \\
&v_i = \frac{\partial u_i}{\partial t} = \dot{u}_i = \omega \partial u_i / \partial \theta \\
&a_i = \frac{\partial v_i}{\partial t} = \ddot{u}_i = \omega^2 \, \partial^2 \, u_i / \partial \theta^2
\end{aligned} \tag{4}$$

Here $\underset{\sim}{r}$ is the position vector of the particle with reference coordinates (r, θ, z), $1 \leq i,j \leq 3$. The time rate of change of $\underset{\sim}{F}$ is

$$\begin{aligned}
\dot{\underset{\sim}{F}} &= \omega \frac{\partial}{\partial \theta} \left\{ \frac{\partial u_i}{\partial r} , \frac{\partial u_i}{\partial \theta} , \frac{\partial u_i}{\partial z} \right\} \quad 1 \leq i \leq 3 \\
&= \omega \frac{\partial}{\partial \theta} \underset{\sim}{F}
\end{aligned} \tag{5}$$

or, since

$$\frac{\partial X_\alpha}{\partial t} = \omega \, \epsilon_{\beta\alpha} \, X_\beta \; , \; \frac{\partial X_3}{\partial t} = 0 \; , \; \alpha, \beta = 1, 2 \tag{6}$$

where $\varepsilon_{\alpha\beta}$ is the two-dimensional permutation symbol ($\varepsilon_{11} = \varepsilon_{22} = 0$, $\varepsilon_{12} = \varepsilon_{21} = -1$), we have

$$\dot{F}^{\alpha}_{\beta} = \omega X_{\gamma}\, \varepsilon_{\gamma\rho}\, u_{\alpha,\rho\beta} \ , \quad 1 \le \alpha, \beta, \gamma, \rho \le 2$$

$$\dot{F}^{3}_{,j} = \dot{F}^{j}_{,3} = 0 \ , \quad j = 1,2,3 \tag{7}$$

where $u_{\alpha,\rho\beta} = \partial^2 u_{\alpha} / \partial X_{\rho}\, \partial X_{\beta}$, and

$$\dot{C}_{\alpha\beta} = \omega\, X_{\gamma} \varepsilon_{\gamma\rho}\, (u_{\mu,\rho\alpha} u_{\mu,\beta} + u_{\mu,\rho\beta}\, u_{\mu,\alpha}) \tag{8}$$

$$\dot{C}_{j3} = 0 \ , \quad 1 \le j \le 3 \ , \quad 1 \le \alpha, \beta, \gamma, \rho, \mu \le 2$$

Thus, time derivatives of such deformation measures are characterized by functions of second derivatives of the motion with respect to the referential coordinates X_i.

The cylinder is assumed to be composed of a viscoelastic material characterized by a constitutive equation for the Cauchy stress $\underset{\sim}{\sigma}$ of the form

$$\underset{\sim}{\sigma} = \underset{\sim}{F}(\underset{\sim}{X};\ \underset{\sim}{C},\ \dot{\underset{\sim}{C}}) \tag{9}$$

where the response functional $\underset{\sim}{F}(\cdot)$ is of a generalized Kelvin-Voight type; e.g.,

$$S_{ij} = G^{1}_{ij}(\underset{\sim}{X}, \underset{\sim}{C}) + \dot{G}^{1}_{ij}(\underset{\sim}{X},\ \dot{\underset{\sim}{C}}) \tag{10}$$

where $\underset{\sim}{S} = \det \underset{\sim}{F}\ \underset{\sim}{\sigma}\ \underset{\sim}{F}^{-T}$ is the Piola-Kirchhoff stress tensor and F^1 and G^2 are response functionals of the deformation and deformation rate, respectively. In certain applications, we may also impose the incompressibility constraint

$$\det \underset{\sim}{F} = 1 \tag{11}$$

VARIATIONAL FORMULATION

Space limitations prevent a full discussion of the derivation of our variational formulation of the rolling contact problem; see reference 1 for more details. It can be demonstrated that the steady-state motion $\underset{\sim}{u}$ of the rolling viscoelastic cylinder satisfies the following nonlinear variational inequality:

$$\underset{\sim}{u} \propto K \ ;$$

$$A(\underset{\sim}{u},\ \underset{\sim}{v} - \underset{\sim}{u}) + j(\underset{\sim}{u},\ \underset{\sim}{v}) - j(\underset{\sim}{u},\ \underset{\sim}{u}) \ge \omega^2\, B(\underset{\sim}{u},\ \underset{\sim}{v} - \underset{\sim}{u}) + f(\underset{\sim}{v} - \underset{\sim}{u}) \tag{12}$$

$$\text{for every } \underset{\sim}{v} \text{ in } k$$

where

$$A(\underset{\sim}{u}, \underset{\sim}{v}) = \text{virtual power}$$

$$= \int_{\Omega} S_{ij}(\underset{\sim}{X}, \nabla \underset{\sim}{u}, \omega)\, v_{i,j}\, dV_0$$

$$j(\underset{\sim}{u}, \underset{\sim}{v}) = \text{the virtual power of the frictional forces}$$

$$= \int_{\Gamma} \nu |\underset{\sim}{S}(\underset{\sim}{X}, \nabla \underset{\sim}{u}, \omega) \cdot \underset{\sim}{n}_0 \cdot \underset{\sim}{i}_2| \; |\underset{\sim}{w}_T(\underset{\sim}{v})| dA_0$$

$$B(\underset{\sim}{u}, \underset{\sim}{v}) = \text{the power developed by inertial forces}$$

$$= \int_{\Omega} \rho_0 \, \partial_\theta \underset{\sim}{u} \cdot \partial_\theta \underset{\sim}{v} \, d V_0$$

$$f(\underset{\sim}{v}) = \text{the virtual power of external forces}$$

$$= \int_{\Omega} \rho_0 \, \underset{\sim}{b} \cdot \underset{\sim}{v} \, d V_0 + \int_{\Gamma_F} \underset{\sim}{t} \cdot \underset{\sim}{v} \, d A_0 \qquad (13)$$

Here Ω is the reference domain in the rigid spinning cylinder, Γ is its exterior (contact) boundary with unit exterior normal $\underset{\sim}{n}_0$, Γ_F is a portion of the boundary on which tractions $\underset{\sim}{t}$ are applied (e.g. pressurization loads), and $S_{ij}(\underset{\sim}{X}, \nabla \underset{\sim}{u}, \omega)$ is the Piola-Kirchhoff stress which is given as a function of $\underset{\sim}{X}$, $\nabla \underset{\sim}{u}$, and $\underset{\sim}{\omega}$ by constitutive laws of the type (10). For example,

$$S_{ij}(\underset{\sim}{X}, \nabla \underset{\sim}{u}, \omega) = {}^{1}_{ij}(\underset{\sim}{X}, \; u_{k,\ell} u_{\ell,k})$$
$$+ {}^{2}_{ij}(\underset{\sim}{X}, \; \omega X_\gamma \varepsilon_{\gamma\rho} u_{\mu,\rho\alpha} u_{\mu,\beta} + u_{\mu,\rho\beta} u_{\mu,\alpha})) \qquad (14)$$

Note that, again, time t does not appear explicitly in this formulation, but the presence of deformation-rate terms in the constitutive equations leads to second derivatives of the motion in the virtual power. In (12), K is the set of admissible motions

$$K = \{ \underset{\sim}{v} = (\omega \, \partial_\theta v_1, \; v_2, \; \omega \, \partial_\theta v_3) \; , \; \underset{\sim}{v} \quad \underset{\sim}{V} \; , \; v^2 \leq H \} \qquad (15)$$

where H is the distance from the axle of the deformed cylinder to the roadway, and V is a space of functions on which the energy is well defined (e.g. $V = W^{2,p}(\Omega)$). In (13), ν is the coefficient of friction, $\underset{\sim}{w}_T = \underset{\sim}{v}_T - v_0 \underset{\sim}{i}_1$ is the slip velocity, v_0 being the speed with which the cylinder moves along the roadway, ρ_0 is the reference mass density, and $\underset{\sim}{b}$ is the body force density.

We reduce (12) to a nonlinear variational equality by regularization: the friction term is regularized by the smoothing scheme discribed in reference 3 (see also ref. 1) and the unilateral contact condition is relaxed by the use of an exterior penalty approximation, as described in reference 1. If the material is incompressible, we also include the incompressibility constraint (11) by the introduction of an appropriate penalty approximation.

SOLUTION OF THE DISCRETE PROBLEM

We now consider finite element approximations of a class of two-dimensional (plane strain) rolling contact problems in which the motion $\underset{\sim}{u}$ is approximated over a mesh of Q_2 (biquadratic) elements. When the regularized version of the variational principle (12) is approximated by finite elements, we obtain a system of nonlinear equations of the form

$$\underset{\sim}{F}(\underset{\sim}{x}, \rho) = \underset{\sim}{0} \tag{16}$$

where $\underset{\sim}{F}$ is an N-vector of nonlinear momentum equations governing the discrete model, $\underset{\sim}{x} = (x_1, x_2, \ldots, x_N)^T$ is a vector of N degrees of freedom representing the nodal values of the motion, and ρ is a parameter representing, for example, the indentation distance H .

We solve (16) using variants of the Riks Keller continuation methods. For example, we regard $(\underset{\sim}{x}, \rho)$ as functions of a real arc-length parameter s , $s \propto [0,1]$, and derive from (10) the system of differential equations,

$$F_i(\underset{\sim}{x}(s), \rho(s)) = 0 \qquad s \propto [0,1] \tag{17}$$

$$\left.\begin{aligned} J_{ij}(\underset{\sim}{x}, \rho)\dot{x}_j + g_i(\underset{\sim}{x}, \rho)\dot{\rho} &= 0 \\ \dot{x}_j \dot{x}_j + \dot{\rho}^2 &= 1 \end{aligned}\right\} \tag{18}$$

where

$$\left.\begin{aligned} J_{ij}(\underset{\sim}{x}, \rho) &= \frac{\partial F_i(\underset{\sim}{x}, \rho)}{\partial x_j} \\ g_i(\underset{\sim}{x}, \rho) &= \frac{\partial g_i(\underset{\sim}{x}, \rho)}{} \\ \dot{x}_j &= \frac{dx_j}{ds} \\ \dot{\rho} &= \frac{d\rho}{ds} \end{aligned}\right\} \tag{19}$$

Equations (17) and (18) hold on the path $\Gamma = \{(\underset{\sim}{x}, \rho) \mid \underset{\sim}{x} = \underset{\sim}{x}(s), \ \rho = \rho(s) , \ 0 \leq s \leq 1\}$ in N+1-dimensional space. Repeated indices are summed from 1 to N. The second member of (18) is, of course, the definition of arc length of Γ .

The system of nonlinear ordinary differential equations (18) is equivalent to the system

$$J_{ij}(\underset{\sim}{x},\ \rho)v_j = g_i(\underset{\sim}{x},\ \rho)$$

$$\dot{\rho}^2 = \frac{1}{1+v_i v_i} \tag{20}$$

$$\dot{x}_j = -\dot{\rho}\, v_j$$

Equations (20) are sufficient to determine directions $(\dot{x}_j, \dot{\rho})$ which define a hyperplane tangent to Γ. These can be used to define a linear extrapolation of the solution into this plane. It then makes sense to correct this approximate solution so that a point on the solution path Γ is obtained. One algorithm for such a procedure is given as follows:

Step 1 (tangent Hyperplane)

With initial data $\underset{\sim}{x}_0$, ρ_0, $(\Delta\rho)_0$, compute

$$J_{ij}(\underset{\sim}{x}_0, \rho_0)v_j^{(1)} = g_i(\underset{\sim}{x}_0, \rho_0)$$

$$\dot{\rho}_i = 1 \Big/ \sqrt{1 + v_j^{(1)} v_j^{(1)}}$$

$$\dot{x}_{1j} = -\dot{\rho}_1\, v_j^{(1)}$$

Step 2 (Extrapolation)

Compute

$$(\Delta s)_1 = (\Delta\rho)_0/\dot{\rho}_1$$

$$\underset{\sim}{x}_1 = \underset{\sim}{x}_0 + \dot{\underset{\sim}{x}}_1(\Delta s)_1$$

$$\rho_1 = \rho_0 + \dot{\rho}_1(\Delta s)_1$$

Step 3 (Correction)

$$J_{ij}^{(r)} w_j^{(r)} = -F_i^{(r)}$$

$$J_{ij}^{(r)} v_j^{(r)} = g_i^{(r)}$$

$$(\Delta\rho)^{(r)} = \frac{-\dot{\underset{\sim}{x}}_1 \cdot \underset{\sim}{w}^{(r)}}{\dot{\rho}_1 - \dot{\underset{\sim}{x}}_1 \cdot \underset{\sim}{v}^{(r)}}$$

$$(\Delta\underset{\sim}{x})^{(r)} = \underset{\sim}{w}^{(r)} - \underset{\sim}{v}^{(r)}(\Delta\rho)^{(r)}$$

with

$$J_{ij}^{(r)} = J_{ij}(\underset{\sim}{x}^r, \rho^r) \ , \ F_i^{(r)} = F_i(\underset{\sim}{x}^r, \rho^r)$$

$$\underset{\sim}{x}^r = \underset{\sim}{x}_1 + \sum_{k=1}^{r} (\Delta \underset{\sim}{x})^{(k)}$$

$$\rho^r = \rho_1 + \sum_{k=1}^{r} (\Delta\rho)^{(k)}$$

$$(\Delta \underset{\sim}{x})^k = \underset{\sim}{x}^{k+1} - \underset{\sim}{x}^k \ ; \ (\Delta\rho)^k = \rho^{k+1} - \rho^k$$

$$1 \leq i,j \leq N \ , \ 1 \leq r \leq R$$

Set

$$\underset{\sim}{x}_1' = \underset{\sim}{x}_1 + \sum_{r=1}^{R} \Delta \underset{\sim}{x}^r = \underset{\sim}{x}^R$$

$$\rho_1' = \rho_1 + \sum_{r=1}^{R} (\Delta\rho)^{(r)} = \rho^R$$

Step 4

Return to Step 1 and continue the process with $(\underset{\sim}{x}_0, \rho_0)$ replaced by $(\underset{\sim}{x}_1', \rho_1')$.

In Step 1, it is, in general, inappropriate to set $(\underset{\sim}{x}_0, \rho_0) = (0, 0)$ since this is not a point on the solution path. The starting point $(\underset{\sim}{x}_0, \rho_0)$ is computed by specifying a small initial value of ρ_0 and computing $\underset{\sim}{x}_0$ by Newton's method.

The procedure in Step 2 was advocated by Keller (reference 4) and has the attractive feature of preserving the symmetry and bandwidth of J_{ij} (when symmetry exists) as opposed to treating the full system (16) at once.

The algorithm given in Step 3 is also a Keller-type scheme, similar in structure to that of Step 2, and is equivalent to the constrained Newton-Raphson scheme,

$$\begin{aligned} J_{ij}(\underset{\sim}{x}^r, \rho^r)\Delta x_j^r + g_i(\underset{\sim}{x}^r, \rho^r)\Delta\rho^r \\ = - F_i(\underset{\sim}{x}^r, \rho_i^r) \\ \dot{\underset{\sim}{x}}_1 \cdot \Delta \underset{\sim}{x}^r + \rho_1(\Delta\rho)^{(r)} = 0 \end{aligned} \qquad (21)$$

The second equation is a constraint on the Newton-Raphson process which forces the scheme to progress toward the solution path Γ in a direction normal to the tangent plane. Some acceleration of this iterative process can be realized by

using alternative constraints which make the iterative scheme follow a spherical path (Crisfield (reference 5)), or an elliptical path (Padovan (reference 6)), and such variants are easily implemented.

Algorithms such as that above can be used to determine limit points and bifurcations in solution paths. Multiple branches can also be determined and followed. While our working program can handle these features, space limitation prevents a discussion of details.

SAMPLE CALCULATION OF A VISCOELASTIC CYLINDER

As a representative example of some of our numerical results, we consider the finite deformation of a viscoelastic cylinder for which the Piola-Kirchhoff stress is given by

$$S_{ij} = \frac{\partial W}{\partial u_{i,j}} + \mu D_{ij}$$

where

$$W = C_1(I_1 - 3) + C_2(I_2 - 3)$$

$$D_{ij} = \tfrac{1}{2}(v_{i,j} + v_{j,i})$$

We choose for the Mooney-Rivlin constants C_1 and the viscosity μ,

$$C_1 = 80 \text{ psi} , \; C_2 = 20 \text{ psi} , \; \mu = 0.0016 \text{ lb sec}^2/\text{in}^2$$

The coefficient of friction is taken to be $\nu = 0.3$ and the density $\rho_0 = 1$. We consider a solid cylinder of initial (undeformed) radius of 2.0 units spinning at an angular velocity $\omega = 5$ rad/sec. The axle load is gradually increased so that contact is made and H is, successively, $H = 1.75$, 1.694, 1.649, 1.600, 1.579, 1.545, and 1.532.

For these choices of parameters, the rolling contact problem was solved using the formulation and methods discussed earlier on a rather coarse mesh of Q_2-biquadratic elements. Computed deformed shapes together with principal stress contours are shown in Figures 2-5 for various values of H and ω. Figure 3 contains the computed variations in maximum stress components with angular velocity ω for a fixed contact length $H = 1.75$ and Figure 4 indicates the variation in axle load with ω for $H = 1.75$. The computed variation of axle load with vertical displacement $d = 2 - H$ is shown in Figure 5. We have also computed contact pressure profiles as a function of H (or F) and ω but do not include these results here.

CORD-REINFORCED RUBBER COMPOSITES

We shall now direct our attention to the construction of a finite element

model of cord-reinforced rubber composites of a type representative of those found in modern pneumatic tires. Two special properties of such composites that influences features of our model are:

i) the ratio of cord to matrix modulus is high (or, in other words, the matrix (rubber) is very soft in comparison with the cord)

ii) the ratio of cord to rubber volume is small

These properties are reflected in a model in which the composite is represented by an anisotropic, Hookean membrane of vanishing thickness attached to a thick layer of isotropic, hyperelastic, rubber matrix (figure 6). The membrane is in a state of plane stress and has no transverse stiffness. Both the membrane and the rubber matrix can withstand finite deformations.

In the models discussed here, the cord membrane element is modelled, using the Gough-Tangorra theory, as an orthotropic sheet with cords oriented at an angle θ, indicated in Figure 6 (see reference 2) and the rubber matrix is assumed to be a Mooney-Rivlin material.

As a sample calculation, consider the reinforced thin cylindrical shell, shown in Figure 7, constructed of two polyester cord layers and a rubber matrix. The end $z = 0$ of the shell element is fixed and the end at $z = H$ is stretched uniformly an amount U in the z-direction. In calculating elasticities of the cord layer using the Gough-Tangorra theory, we take d = number of cord ends/cm = 102 and E_c = Young's modulus = 3.97 GPa while the matrix is a 60NR/40 SBR rubber with a Young's modulus $C_1 + C_2 = 5.5$ MPa. Other dimensions are given in Figure 7.

Since this composite element can undergo finite extensions, the "optimum" cord angle θ^* (the ply angle corresponding to a minimum axial force F_z for a given stretch U/H) may vary with deformations. To study this behavior, we have calculated solutions to finite element approximations of this problem for values of $\theta = 0^\circ, 10^\circ, 20^\circ, \ldots, 90^\circ$ and U/H of 1% to 20%.

It is first noted that stretching of the sheet changes the cord angle orientation throughout the specimen. The amount of angle change $\nabla\theta$ depends upon the initial orientation θ and the amount of stretch, and for $U/H = .10$ and the material properties assumed, the maximum change occured for an orientation of $\theta = 70^\circ$, as indicated in Figure 7b.

One problem of practical interest is to determine θ for given U/H, the value of θ at which the inter-laminar shear stress τ is minimized. For the example computed here, τ was found to be zero for $U/H = .10$ at a ply angle of around 35° (see Figure 8). The results of other calculations are illustrated in Figures 9 and 10. The total cord force versus cord angle for various stretches is illustrated in Figure 9 while the net axial force F_z for various cord angles and stretches is given in Figure 10. It is interesting to note that the minimum F_z is roughly independent of the amount of stretch and occurs for a ply angle of around $\theta \approx 35^\circ$.

We have performed similar calculations for reinforced shell elements subjected to internal radial pressures, simulating pressurization of a tire. Because of space limitations, these results are not given here.

REFERENCES

1. Oden, J.T.; Becker, E.B.; Lin, T.L.; and Demkowicz, L.: Formulation and Finite Element Analysis of a General Class of Rolling Contact Problems with Finite Elastic Deformations. Mathematics of Finite Elements with Applications, Vol. V, edited by J.R. Whiteman, Academic Press Ltd., London, 1984.

2. Walter, J.D.: Cord Reinforced Rubber Section 3.1, Mechanics of Pneumatic Tires, Revised Edition; edited by S.K. Clark, U.S. Dept. of Transportation, Washington, D.C., 1981, pp. 123-177.

3. Campos, L.T.; Oden, J.T.; and Kikuchi, N.: A Numerical Analysis of a Class of Contact Problems with Friction in Elastostatics, Comp. Meth. in Appl. Mech. & Engrg. 34, 1982, pp. 821-845.

4. Keller, H.B.: Practical Procedures in Path Following Near Limit Point, in Computing Methods in Applied Sciences and Engineering, R. Glowinski and J.L. Lyons, eds., North-Holland Publ. Inc., 1982.

5. Crisfield, M.A.: A Fast Incremental/Iterative Solution Procedure that Handles 'Snap-Through', Comput. & Struct. 13, 1981, pp. 55-62.

6. Padovan, J. and Arechaga, T.: Formal Convergence Characteristics of Elliptically Constrained Incremental Newton-Raphson Algorithms, Int. J. Eng. Sci. 20(10), 1982, pp. 1077-1097.

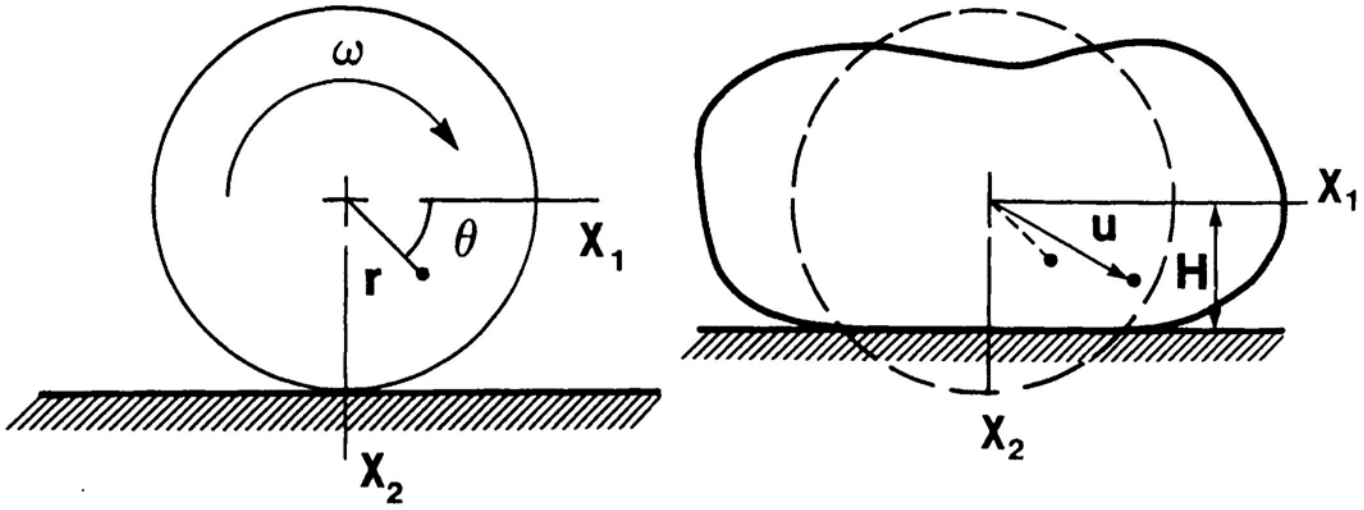

Figure 1. Finite deformation of a rolling viscoelastic cylinder.

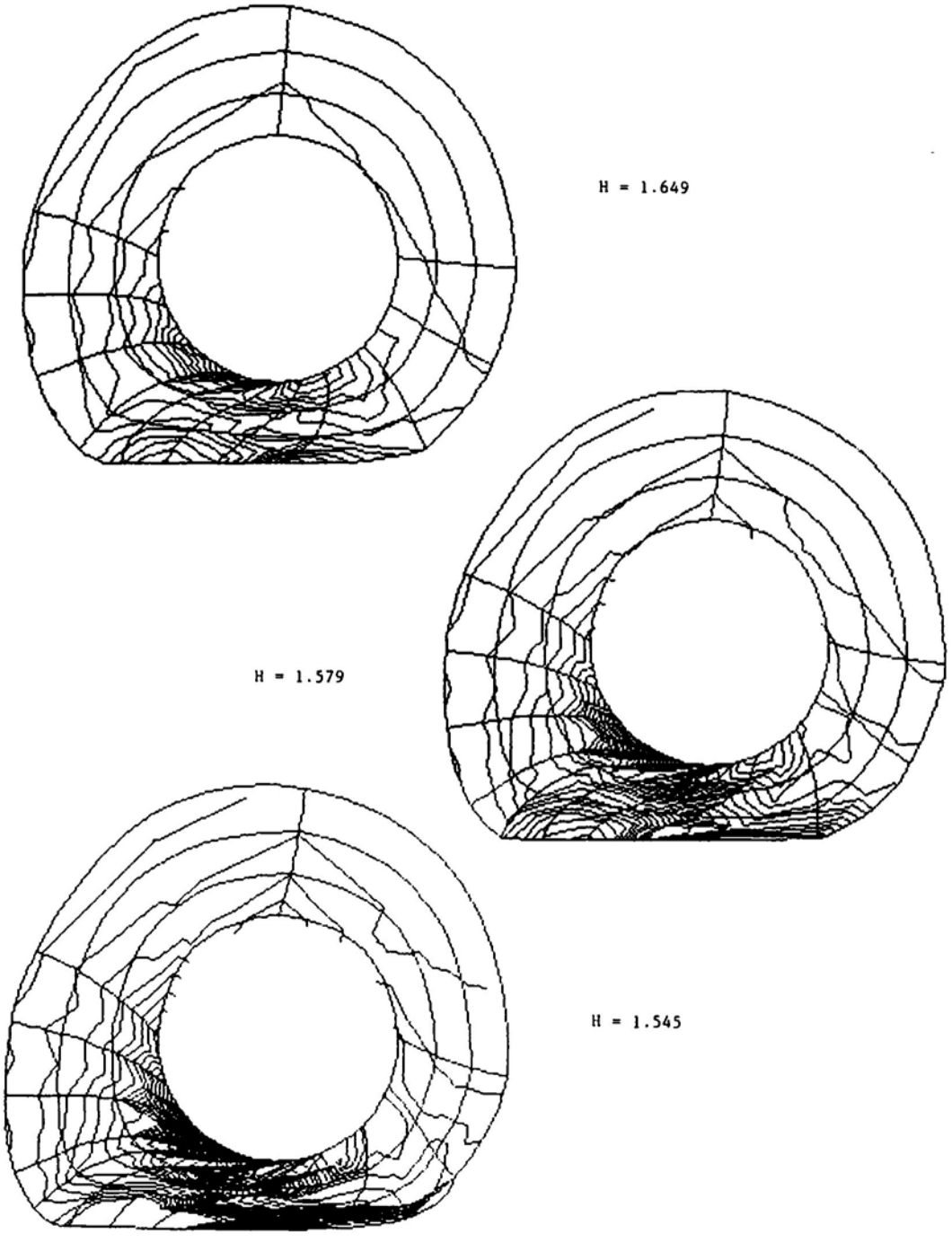

Figure 2. Computed generated deformed shapes and stress contours for viscoelastic cylinder.

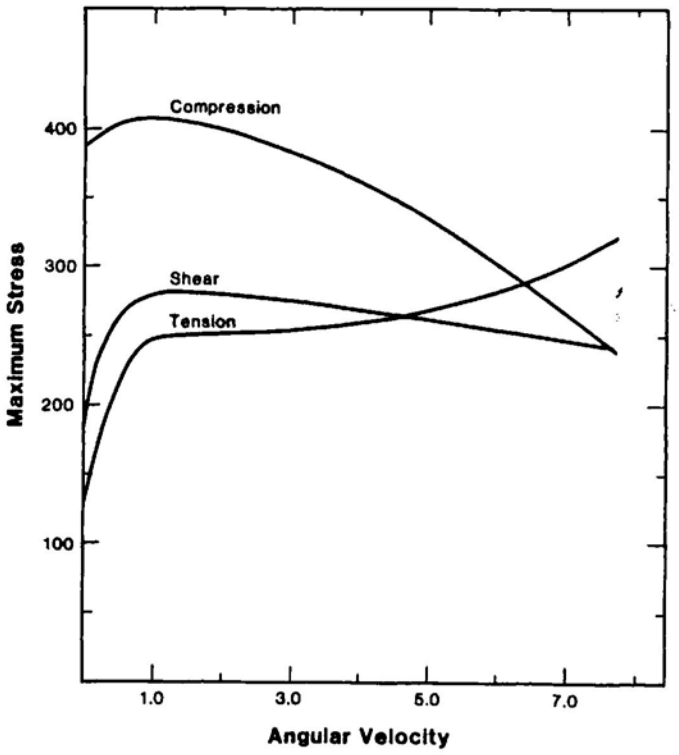

Figure 3. Maximum stress variation with angular velocity (rad/sec).

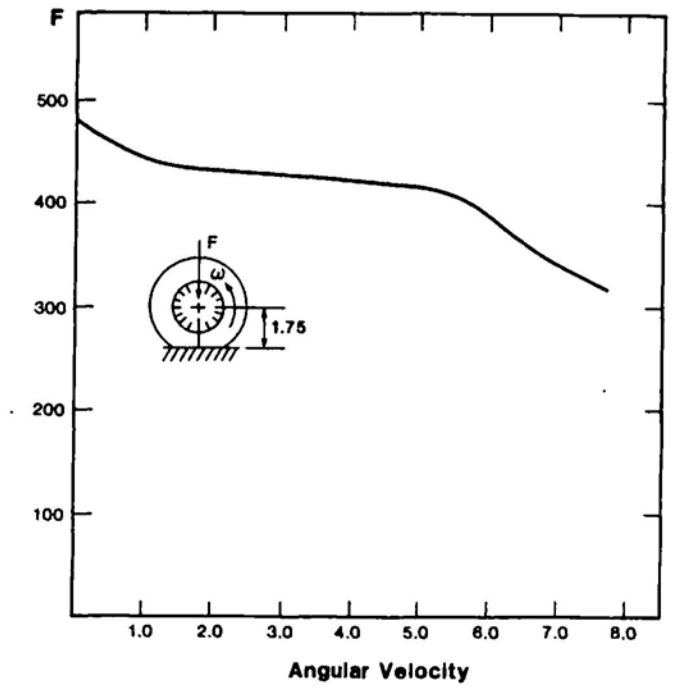

Figure 4. Axle load versus angular velocity (rad/sec).

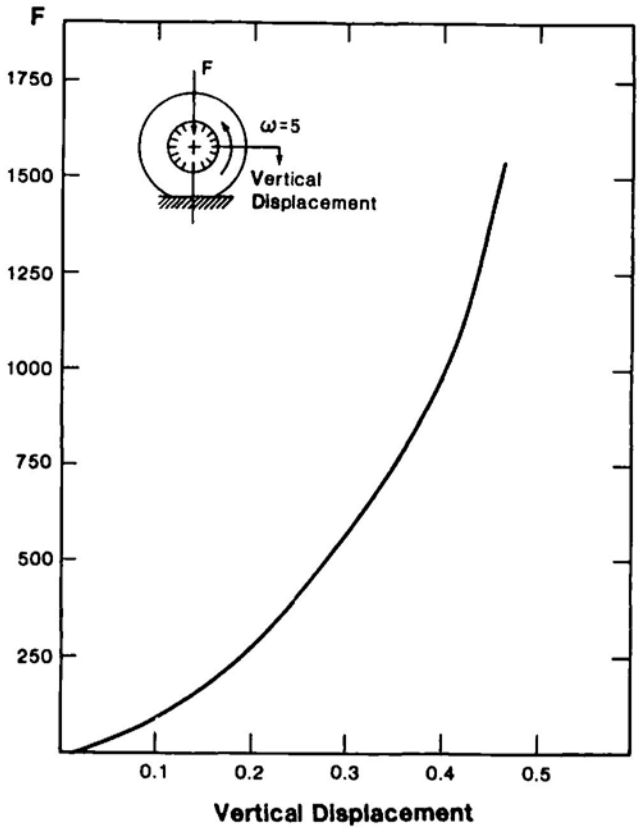

Figure 5. Axle load F versus displacement d = 2.0 - H.

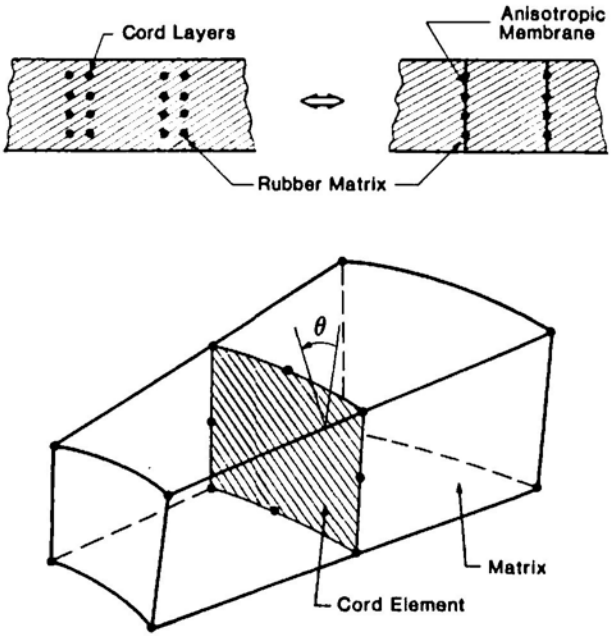

Figure 6. Model of a cord-reinforced rubber composite.

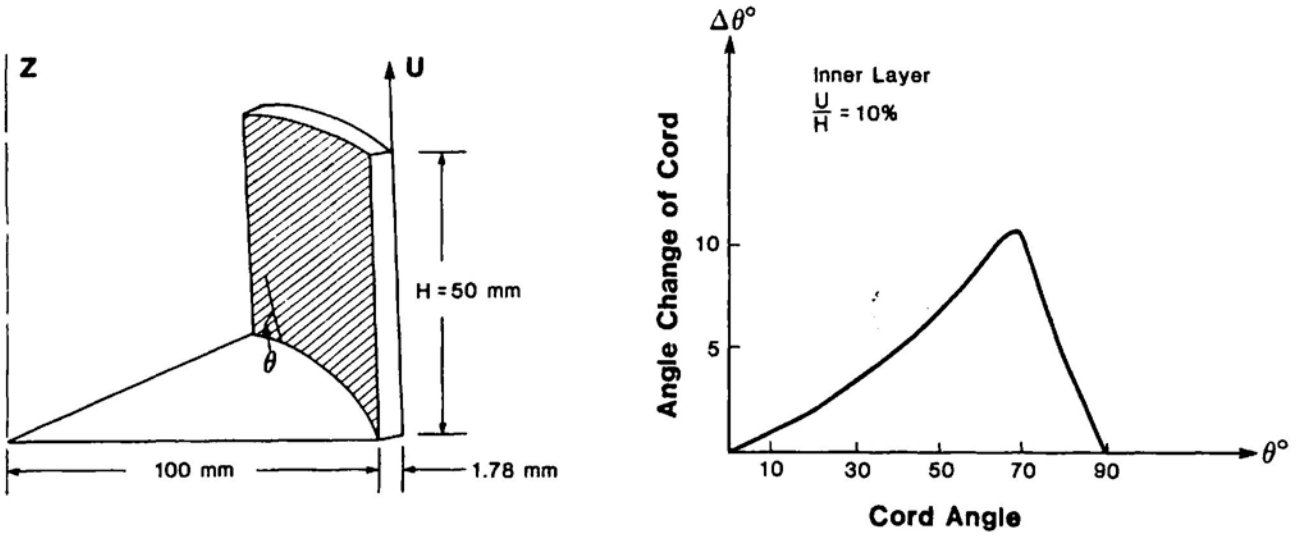

(a) A cord-reinforced shell.

(b) Change in cord angle due to stretching.

Figure 7. Reinforced thin cylindrical shell.

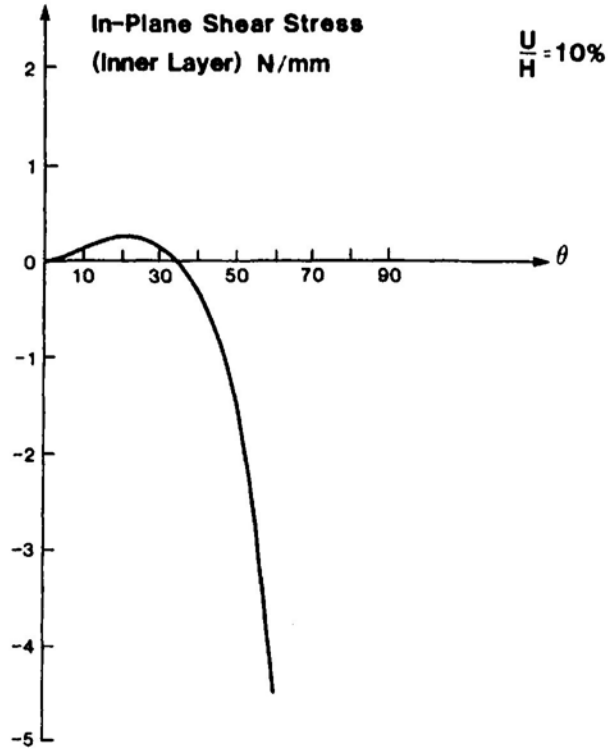

Figure 8. Interlaminar shear stress as a function of cord angle for U/H = .10.

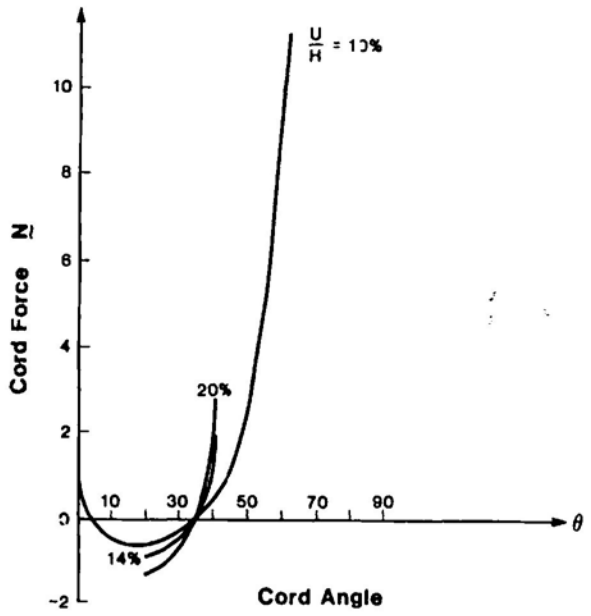

Figure 9. Computed variation of cord force N with cord angle for different stretch ratios.

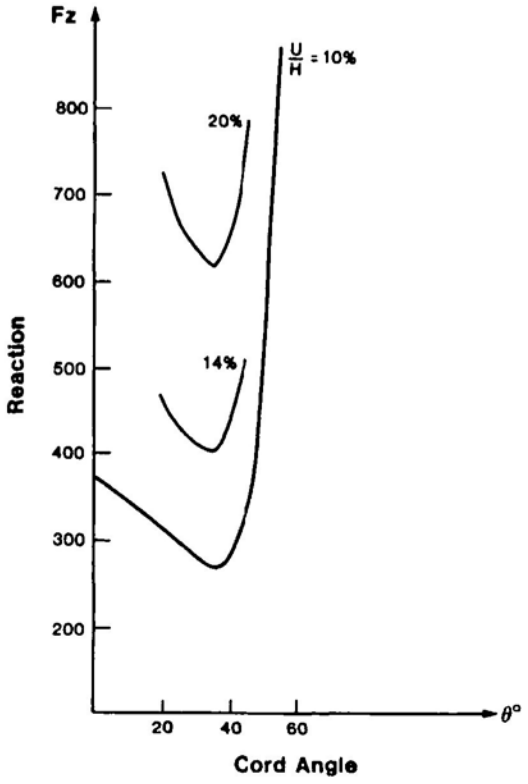

Figure 10. Calculation of dependence of axial stiffness for various cord angles at different stretch ratios.